Review

Design and Experimental Analysis of an Adhesive Joint for a Hybrid Automotive Wheel

Jens-David Wacker [1,*], Tobias Kloska [2], Hannah Linne [3], Julia Decker [1], Andre Janes [2], Oliver Huxdorf [3] and Sven Bose [2]

[1] Fraunhofer Institute for Structural Durability and System Reliability LBF, 64283 Darmstadt, Germany
[2] OTTO FUCHS KG, 58540 Meinerzhagen, Germany
[3] INVENT GmbH, 38112 Braunschweig, Germany
* Correspondence: jens-david.wacker@lbf.fraunhofer.de; Tel.: +49-6151-705-8356

Abstract: When it comes to lightweight design of automotive wheels, hybrid designs consisting of a carbon composite wheel rim and a metallic, e.g., aluminum alloy, wheel disc offer significant potential. However, the conventionally used bolted joint between the two parts is complex and requires compromises in lightweight design due to the additional mechanical elements. Within this research, an adhesive joint for a hybrid wheel is developed in order to demonstrate its performance and lightweight potential. The main challenges are the reliable resistance against high structural loads during different load cases, as well as the residual stresses in the joint due to different thermal expansion rates of the composite and aluminum material. The developed joint combines an adhesive bond with a form-fitted geometry while still enabling an assembling process of the wheel disc in rotational direction. In addition, adaptations of the fiber layup in the rim area significantly reduce the thermal residual stresses in the joint by 47%. Subcomponent specimens, which represent the joint of an aluminum spoke with the composite rim, are manufactured and tested at different temperatures and load cases. The test results show sufficient strength of the adhesive joint as well as an improvement of the developed form-fitted joint compared to a basic adhesive bond. The adhesively joined wheel offers a lightweight potential of 6% compared to the bolted wheel.

Keywords: adhesive joint design; hybrid joint; lightweight wheel; composites; thermal expansion; experimental analysis; structural analysis

1. Introduction

Hybrid automotive wheels, consisting of a carbon composite (CFRP) wheel rim and an aluminum alloy wheel disc, have been state of the art for several years, offering a lightweight potential of 15 to 20% compared to monolithic aluminum wheels [1–4]. The large wheel rim represents the greatest portion of the wheel. Therefore, its composite design effectively reduces the rotational mass and improves the damping behavior of the wheel. In addition, the cylindrical geometry enables more efficient manufacturing processes such as braiding [5] and resin transfer molding [6,7], offering advantages regarding mass production compared to full composite wheels. The wheel disc with its complex spoke design, on the other hand, is best realized in metal manufacturing processes such as casting or forging [8], with high strength and fatigue values and precise processing of the hub intersection. The joint between the two parts is conventionally realized as a bolted joint [9,10], due to the high structural and thermal loads. However, the realization of bolted joints is complex. Milling processes of the composite part and integration of threaded holes in the aluminum disc are necessary, as well as sealing measures. In addition, the bolted joint usually needs to be combined with a form-fitted sleeve design as resistance against the high resulting shear loads. These additional mechanical elements lead to compromises in lightweight design.

Within this federal research project [11], an adhesive joint for a hybrid automotive wheel is developed in order to demonstrate its performance and lightweight potential. In general, adhesive bonds offer several advantages when it comes to joining metal and composite parts. The load introduction into the composite part can be realized without damaging fiber structures, dimensional deviations of the parts can be compensated in the adhesive thickness, and the overall mass of the joint can be reduced [12,13], (pp. 2–4). In case of a hybrid wheel, the joint design faces several challenges. As a safety component, the reliable resistance against high structural loads during different load cases such as straight driving, cornering, accelerating, and braking must be assured, as well as electric conductivity and resistance to ageing. In addition, the materials must withstand a large temperature range from low ambient temperatures to high braking temperatures. In case of composite wheels, measures to shield the wheel components from the braking heat are usually taken, such as coatings or layers for heat reflection, heat distribution or insulation [14,15]. However, the high temperature difference still leads to residual stresses in the joint, due to the different thermal expansion rates of the composite and aluminum material, and needs to be considered in the design process.

In the review of literature, several design parameters regarding adhesive bonding of dissimilar materials can be identified. Apart from the selection of adhesive and adherend material with suitable mechanical properties [12], (pp. 694–696), the geometrical design of the joint has a significant influence on the stresses in the adhesive and adherend, e.g., a single-lap design compared to a double-lap design [12], (pp. 713–714). In [16], a review on design techniques to improve the strength of adhesive joints is given. Examples are form-fitted configurations such as a wavy adherend design, transverse reinforcements such as pinning or stitching, or specific design of the adhesive edges such as adherend tapers or adhesive fillets. In addition, dual-adhesive concepts can be used [13], combining a high-temperature and a low-temperature adhesive. The hybrid wheel, however, demonstrates a more unique application compared to the often described overlap joints in the literature, due to its circular geometry, its specific deformation during thermal expansion, and loading situation.

When developing adhesive joints, computational and experimental methods are commonly used for structural validation. In the case of hybrid joints, different failure modes need to be considered. Apart from cohesive failure of the adhesive, several studies with composite adherends show delamination of the surface layer within the joint area, dependent, e.g., on the load introduction or thermal exposure of the joint [17–19].

Figure 1 shows the test program for the hybrid joint development for the research. Material properties for the simulation models are evaluated using coupon specimens [20,21]; the hybrid bond is validated on single lap joints [22]. Tests on subcomponent specimens first give experimental joint validation, and tests on wheel prototypes give validation on a component level.
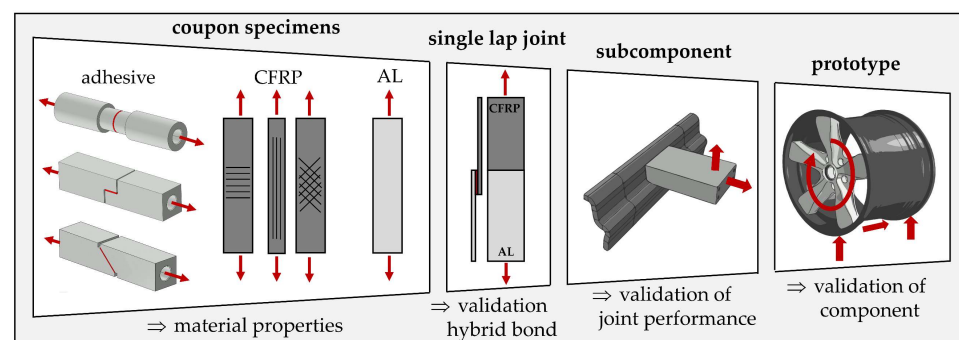

Figure 1. Test program for the experimental validation of the hybrid adhesive joint.

This paper elaborates on the preliminary design development of the hybrid adhesive joint and its first experimental validation on the subcomponent level. This includes
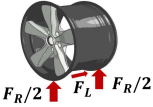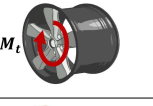
the analysis of requirements, material selection, geometrical joint design, as well as the manufacturing and testing of subcomponent specimens. Other related topics, such as the characterization of the adhesive and adherend materials, structural simulation and strength analysis of the adhesive and adherends, as well as elaborations on the manufacturing concept of the wheel, may be presented in future publications.

2. Design of an Adhesive Joint for the Hybrid Wheel

2.1. Wheel Requirements

For the research, a 11.5 J × 20 EH2 ET 56 hybrid wheel with a five-spoke design and a max. wheel load of 575 kg was chosen as the reference wheel. In order to identify specific structural requirements for the joint, the different wheel load cases need to be considered. Within Table 1, the load cases such as straight driving, cornering, braking/accelerating and their respective maximum load values are listed. Maximum radial loads occur during straight driving, with maximum lateral load during cornering and maximum torsional moment during braking or accelerating, and equal values in opposite directions. Maximum temperature within the wheel rim is defined as 200 °C and within the joint as 150 °C, due to the greater distance to the brake. Lowest ambient temperature is defined as −40 °C.

Table 1. Load requirements for the hybrid wheel within the research project [11] according to OTTO FUCHS KG and Fraunhofer LBF.

No.	Load Case	Load	Value	Unit	Sketch
L1	straight driving (incl. rough road driving)	max. radial load	14.02	kN	
		max. lateral load	3.84	kN	
L2	cornering	max. radial load	10.59	kN	
		max. lateral load	12.71	kN	
L3	braking/ accelerating	max. torsional moment	±1.91	kNm	
L4.1	thermal loading	max. temperature joint	150	°C	
L4.2		min. temperature joint	−40	°C	
L4.3		max. temperature wheel rim	200	°C	

For the objective of this research, the evaluations are limited to the selection of load cases listed in Table 1. The consideration of further combinations of load cases and temperatures can be addressed in a future detailed design stage.

2.2. Material Selection

Main requirements for the selection of materials for the hybrid wheel are high structural performance as well as thermal and corrosion resistance.

The adhesive selected for the project is a newly developed, one-component, heat-curing, epoxy-based structural adhesive by the associated project partner DuPont Specialty Products GmbH & Co KG. It has a high glass-transition temperature of 174 °C and a good capability of bonding dissimilar materials such as composites and metals. The adhesive will be further labeled as "BETAMATE™ HTG".

The aluminum alloy chosen for the wheel disc is EN AW-6082 T6 [23], a standard forging alloy by OTTO FUCHS KG with high strength and good corrosion resistance.

When it comes to selecting the composite material, the manufacturing process needs to be considered. As fabric, bidirectional woven carbon fabric WELA GG-245-1000T [24] is used, offering advantages regarding draping of complex geometries compared to non-

crimp fabrics. Local reinforcements are realized with unidirectional carbon fiber WELA GV-303-0500UTFX [25]. The selected resin system is Araldite® LY 1560 [26], a toughened epoxy resin with a high glass-transition temperature of 205 °C, made for resin transfer molding (RTM) or infusion.

2.3. Analysis of Joint Requirements

The wheel loads described in Table 1 are introduced into the wheel at the tire–wheel intersection and are supported by the wheel hub. The load distribution within the wheel depends on the load case and the orientation of the spokes during the 360° rollover. In order to identify the critical loads occurring at the joint intersections, a finite element (FE) simulation using Ansys Workbench 2020 R1 software is carried out. The objective is the analysis of joint requirements by evaluating critical force and moment resultants within the joint.

2.3.1. Finite Element Model

The joint is modeled as a "basic joint", in which the outer surfaces of the aluminum spokes are joined with the wheel rim by a simple adhesive layer, as shown in Figure 2a. The composite rim with its specific fiber layup is modeled using Ansys Composite PrepPost (ACP) with shell elements. The aluminum disc, as well as the adhesive layer are modeled with solid elements. The material behavior is defined as linear elastic, using material data partly generated on coupon specimens within the project by Fraunhofer LBF. The most important material parameters are listed in Table 2.

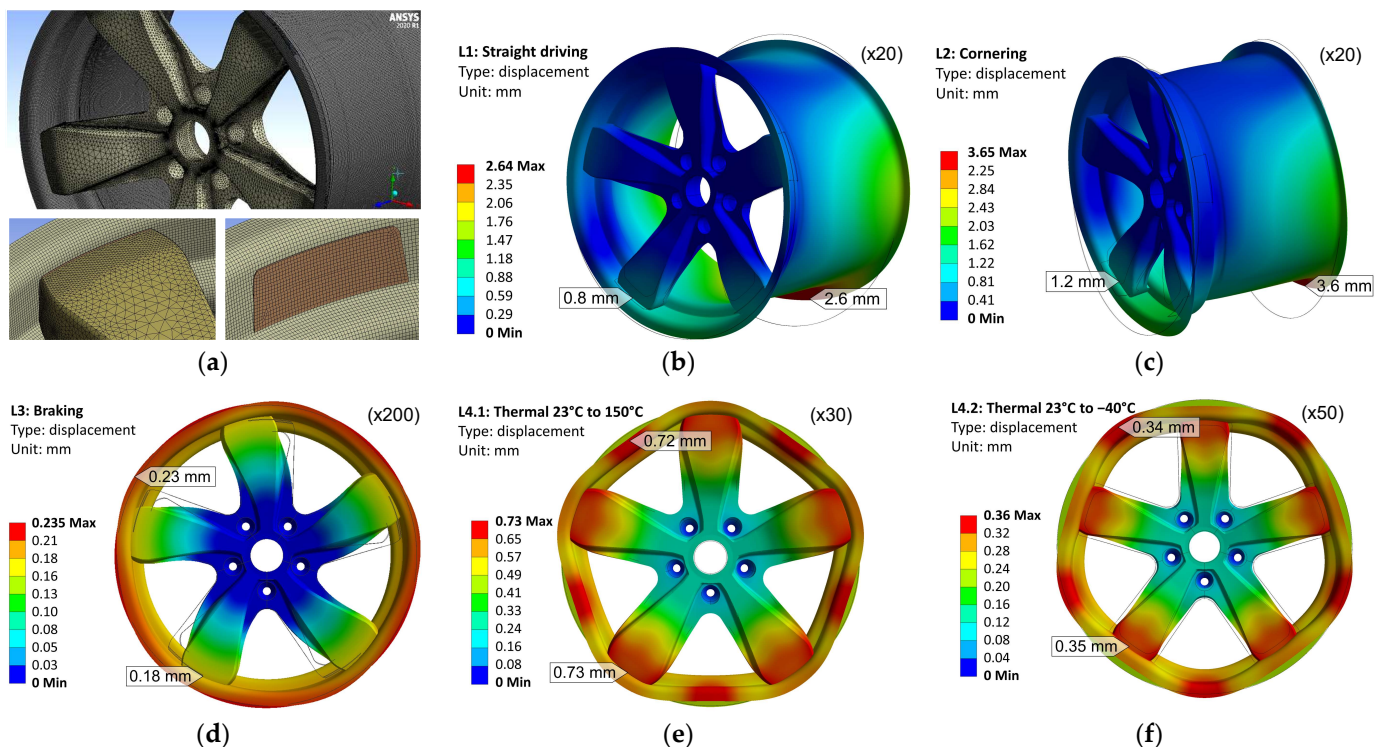**Figure 2.** Simulation of the hybrid wheel in different load cases: (**a**) finite element model of wheel and joint with adhesive layer; (**b**) wheel displacement during L1: straight driving; (**c**) displacement during L2: cornering; (**d**) displacement during L3: braking; (**e**) displacement during L4.1: thermal load case 23 to 150 °C; (**f**) displacement during L4.2: thermal load case 23 to −40 °C.

Table 2. Selection of material parameters (for room temperature) used for linear elastic simulation of the hybrid wheel for the analysis of force and moment resultants within the joint.

Carbon/Epoxy Composite Orthotropic Ply WELA GG-245 [24]/ Araldite® LY 1560 [26]			Carbon/Epoxy Composite Unidirectional Ply WELA GV-303-0500 [25]/ Araldite® LY 1560 [26]			Aluminum Alloy, Isotropic EN AW-6082 T6 [23]			Adhesive, Isotropic BETAMATE™ HTG		
Property	Value	Unit	Property	Value	Unit	Property	Value	Unit	Property	Value	Unit
E_x	66.39 [1]	GPa	E_x	124.24 [1]	GPa	E	70.00 [3]	GPa	E	2.54 [1]	GPa
E_y	66.39 [1]	GPa	E_y	8.78 [1]	GPa	ν	0.33 [3]	-	ν	0.40 [4]	-
G_{xy}	15.76 [1]	GPa	G_{xy}	4.70 [2]	GPa	α	23.4 [3]	10^{-6}/K	α	40.0 [4]	10^{-6}/K
ν_{xy}	0.30 [1]	-	ν_{xy}	0.27 [2]	-						
α_x	2.2 [2]	10^{-6}/K	α_x	−0.5 [2]	10^{-6}/K						
α_y	2.2 [2]	10^{-6}/K	α_y	30.0 [2]	10^{-6}/K						

[1] data determined in coupon tests by Fraunhofer LBF. [2] data from similar material within Ansys Workbench 2020 R1 data base. [3] data from product data sheet [23]. [4] data according to DuPont Specialty Products GmbH & Co KG (Macquarie Park, Australia).

2.3.2. Wheel Deformation in Different Load Cases

For the interpretation of the structural behavior of the joint, examination of the simulated wheel deformation of the different load cases is helpful, as shown in Figure 2b–f.

The load cases "L1: straight driving" (Figure 2b) and "L2: cornering" (Figure 2c) lead to asymmetrical deformation of the wheel with a maximum deformation of 2.6 mm in L1 and 3.6 mm in L2 on the inboard side of the wheel rim. Deformations greater than 5 mm can result in critical tyer leakage. The outboard side of the wheel is less deformed, due to the stiffness of the aluminum wheel disc. However, especially in the case of "cornering", the high lateral load leads to maximum deformation of the spoke of 1.2 mm.

The load case "braking" (Figure 2d) is rotationally symmetrical, due to the symmetrical introduction of the torsional moment. Only little deformation of max. 0.23 mm occurs in this load case.

For the thermal load cases, a stress neutral temperature at 23 °C is assumed, without consideration of possible residual stresses from the manufacturing process. The temperature rise in "L4.1: Thermal 23 to 150 °C" (Figure 2e) leads to an expansion of the wheel components. Due to the greater thermal expansion rate of the aluminum alloy compared to the composite material, the wheel disc compresses the wheel rim into a polygon-like shape with a maximum deformation of 0.73 mm. The temperature drop in "L4.2: Thermal 23 to −40 °C" (Figure 2e) leads to a greater contraction of the wheel disc, pulling the wheel rim interfaces toward the center axis. Here, the maximum deformation is 0.35 mm.

2.3.3. Force and Moment Resultants within the Joint

In order to evaluate the critical force and moment resultants within the joint, different spoke positions during the 360° rollover need to be considered. Therefore, each load case is simulated in different orientations of the wheel, allowing for a joint evaluation in 18° increments along the 360° rollover. The force and moment resultants are evaluated at the intersection between the outer surface of the aluminum spoke and the inner surface of the adhesive layer, as shown in Figure 3a. The resultants are orientated in a cylindrical coordinate system with a radial (R), lateral (L) and circumferential (φ) direction. A positive radial force resultant $+F_R$ can be interpreted as tensional loading of the adhesive layer, a negative radial force resultant $−F_R$ as compression loading.

An exemplary evaluation of the force and moment resultants over the 360° wheel rollover for the load case "L2: cornering" is shown in Figure 3b,c. The graphical course shows maxima and minima in different spoke positions. Extreme radial and lateral forces occur at 180° spoke position, with extreme circumferential forces as well as all extreme moment resultants at 126° and 234° spoke position.
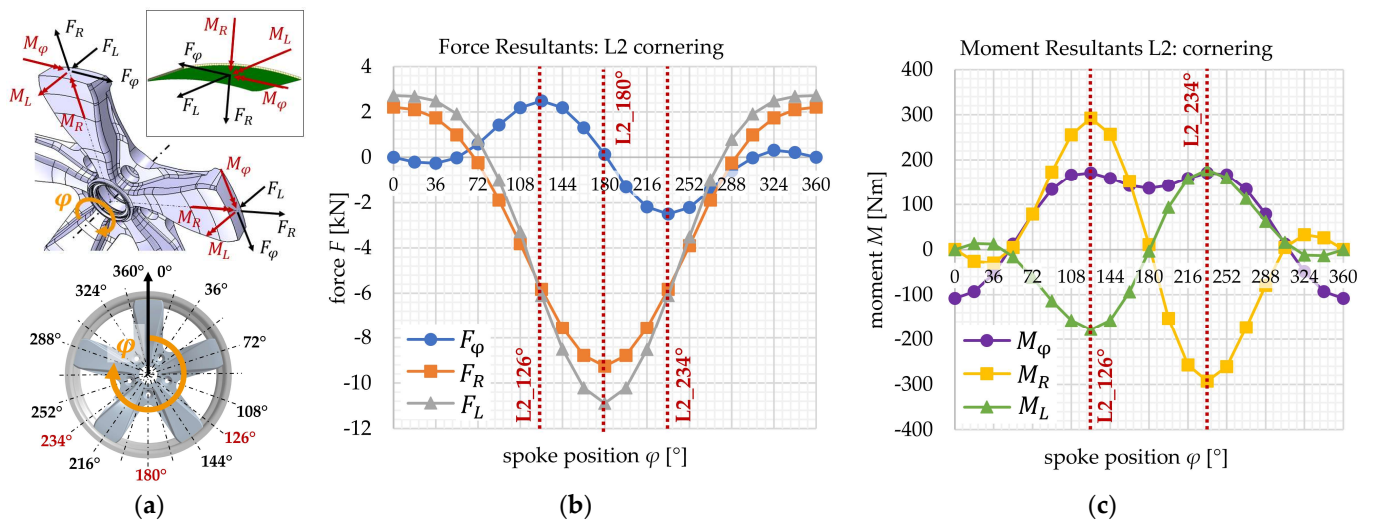
Figure 3. (**a**) Visualization of force and moment resultants at the intersection between the spoke and the adhesive layer during 360° rollover; (**b**) force resultants for the load case "L2: cornering"; (**c**) moment resultants for the load case "L2: cornering".

In Table 3, the selected critical force and moment resultants for each load case are listed, evaluated from the respective extrema in the 360° rollover. In the load case "L1: straight driving", maximum force resultants within the joint occur at 180° spoke position, with maximum moment resultants at 126° and 234°, similar to the load case "L2: cornering". However, the load values during cornering appear to be more extreme, with a high radial force resultant of −9.25 kN and a high lateral force resultant of -10.89 kN. The high radial moment resultants of 293 Nm can be explained by to the deformation reaction of the spoke, caused by the circumferential force resultant of 2.50 kN. Due to the open C-shaped cross-section of the spoke, the resulting bending deformation is coupled by a drilling deformation around the radial axis.

Table 3. Selection of critical force and moment resultants within the wheel joint for different load cases and spoke positions.

No.	Load Case	Spoke Position	Force Resultants			Moment Resultants		
			F_φ (kN)	F_R (kN)	F_L (kN)	M_φ (Nm)	M_R (Nm)	M_L (Nm)
L1	straight driving	126°	0.87	−3.67	−2.84	88	193	−205
		180°	0.08	−8.39	−6.64	43	8	−5
		234°	−0.87	−3.67	−2.84	88	−193	205
L2	cornering	126°	2.50	−5.83	−6.10	171	293	−178
		180°	0.13	−9.25	**−10.89**	136	11	−3
		234°	−2.50	−5.83	−6.10	171	−293	178
L3	braking	all pos.	−1.52	0	0	0	−78	9
L4.1	23 to 150 °C	all pos.	0	−28.61	0.02	−67	0	0
L4.2	23 to −40 °C	all pos.	0	**14.08**	−0.01	33	0	0

The same effect can be observed in the load case "L3: braking". The braking torque leads to a circumferential force resultant of −1.52 kN within the joint, which then results in a radial moment resultant of −78 Nm, due to the spokes' cross-sectional design. However, the braking load condition appears to be less critical for the joint, with significantly lower load values compared to the other load cases.

The thermal load cases lead to high residual radial force resultants, as described before. The temperature rise in "L4.1: Thermal 23 to 150 °C" leads to radial force resultants of

−28.61 kN, and the temperature drop in "L4.2: Thermal 23 to −40 °C" of +14.08 kN shows far more extreme values than in the other load cases.

When developing the adhesive joint for the hybrid wheel, all force and moment resultants and their interactions need to be considered as structural requirements. The resulting stress state within the adhesive layer depends on the final chosen geometrical design of the joint area. However, the evaluation of the principal stresses of the adhesive layer of this preliminary "basic design" give first conclusions about the joint loading:

- The high radial force resultant of +14.08 kN in L4.2 leads to critical tensional loading of the joint, due to the significantly lower tensional strength compared to the compressional strength of the adhesive.
- The high lateral force resultant of −10.89 kN in L2 leads to critical shear loading.
- The circumferential and lateral moment resultants M_φ and M_L can be considered more critical than the radial moment resultant M_R, because they lead to out-of-plane pealing stresses rather than in-plane shear stresses within the adhesive layer.
- The braking/accelerating load case can be considered as the least critical load case, resulting in rather low stress states.

2.4. Joint Design

For the development of the adhesive joint design, several concepts considering the review of literature are generated, analyzed via finite element simulation and evaluated according to their estimated structural performance, reliability, manufacturability and lightweight potential. The concepts include different approaches regarding design parameters such as geometrical design, material selection, bonding direction, as well as adaptations of the rim and spoke design. The final selected design features two main characteristics, which are elaborated in the following:

- the adaption of the fiber layup in the composite rim flange;
- the geometrical joint design with a form-fitted radial and lateral support.

2.4.1. Adaption of the Fiber Layup for the Composite Rim

The analysis of the joint requirements shows that critical radial force resultants occur in the thermal load cases due to the different thermal expansion rates of the aluminum wheel disc and the composite wheel rim. In the case of the composite rim, the thermal expansion rate as well as the rim stiffness result from the fiber layup and therefore offer the potential of more convenient design adaptations. In the original rim design (Figure 4a), unidirectional reinforcements are inserted in the rim flange areas with the objective of increasing the rim stiffness in the circumferential direction, as well as realizing thicker areas with a specific surface geometry. However, the reinforcements are primarily necessary for the in-board flange side. On the out-board side, the aluminum wheel disc increases the rim stiffness. This allows for the replacement of the unidirectional reinforcements with foam core segments (Figure 4b), while still achieving sufficient strength and stiffness of the rim flange. This sandwich design leads to a more flexible behavior of the rim flange in circumferential directing, as well as to a reduction of the difference in thermal expansion between the composite and aluminum components.

Figure 4c,d show the changes in deformation behavior between the original and the adapted design for the load case "L4.2: Thermal 23 to −40 °C". In both variations, the shrinkage of the aluminum disc due to the temperature drop is similar. The deviation of the composite rim to its undeformed shape, on the other hand, is less pronounced in the adapted variation, with only a 0.25 mm deviation between the spokes, compared to 0.35 mm in the original design.
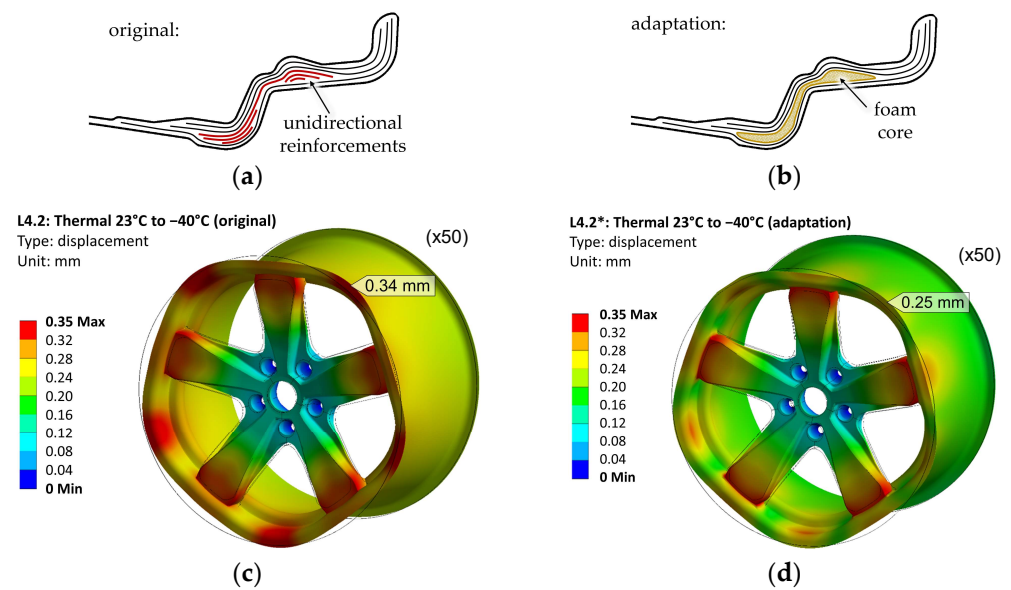
Figure 4. (**a**) Sketch (no detailed design) of the original fiber layup of the out-board rim flange with unidirectional reinforcements; (**b**) sketch of the adapted fiber layup with foam core; (**c**) deformation plot of original design under thermal load 23 to −40 °C; (**d**) deformation plot of adapted design.

Table 4 contains the force and moment resultants for the thermal load cases L4.1* and L4.2*, evaluated with the new design adaptation in the rim flange. The evaluation shows a significant reduction of the radial force resultants by 47%, with −15.18 kN instead of the former −28.61 kN in L4.1, and 7.47 kN instead of the former 14.08 kN in L4.2. Therefore, the design adaptation significantly improves the load requirement for the joint design.

Table 4. Force and moment resultants within the wheel joint for the thermal load cases, evaluated with the design adaptation in the rim flange.

No.	Load Case	Spoke Position	Force Resultants			Moment Resultants		
			F_φ (kN)	F_R (kN)	F_L (kN)	M_φ (Nm)	M_R (Nm)	M_L (Nm)
L4.1 *	23 °C to 150 °C	all pos.	0	−15.18	−0.10	53	0	0
L4.2 *	23 °C to −40 °C	all pos.	0	**7.47**	0.05	26	0	0

* Evaluated from model with design adaptation in the out-board rim flange.

Further investigation of the other load cases "L1*: straight driving", "L2*: cornering", and "L3*: braking" with the new design adaptation shows no significant change in force and moment resultants. This can be explained due to the rather force-controlled loading in these load cases, instead of the rather deformation-controlled loading in the thermal load cases.

2.4.2. Geometrical Joint Design

As a critical structural component, the hybrid wheel has high requirements regarding safety and reliability. In the case of adhesive joints, the combination of an adhesive bond with a form-fitted design can improve the joint performance and reduce critical tensional or pealing stresses, as well as enable a fail-safe mechanism in case of adhesive failure. However, the realization of a form-fitted adhesive design requires consideration of the bonding process, e.g., the application of the adhesive and the bonding direction.

Within an iterative design process, considering structural finite element analyses and manufacturing limits, a geometrical joint design is developed, in which a form-fitted radial and lateral support is implemented, as shown in Figure 5. The design is realized by adaptation of the foam core segments in the rim flange in the joint areas. The cross-sectional

view shows the "claw-like" fit of the joint, supporting the adhesive bond regarding critical radial and lateral force resultants F_R and F_L, as well as radial and lateral moment resultants M_R and M_L. The overall design of the adhesively joined wheel offers a lightweight potential of 6% compared to the bolted hybrid wheel.
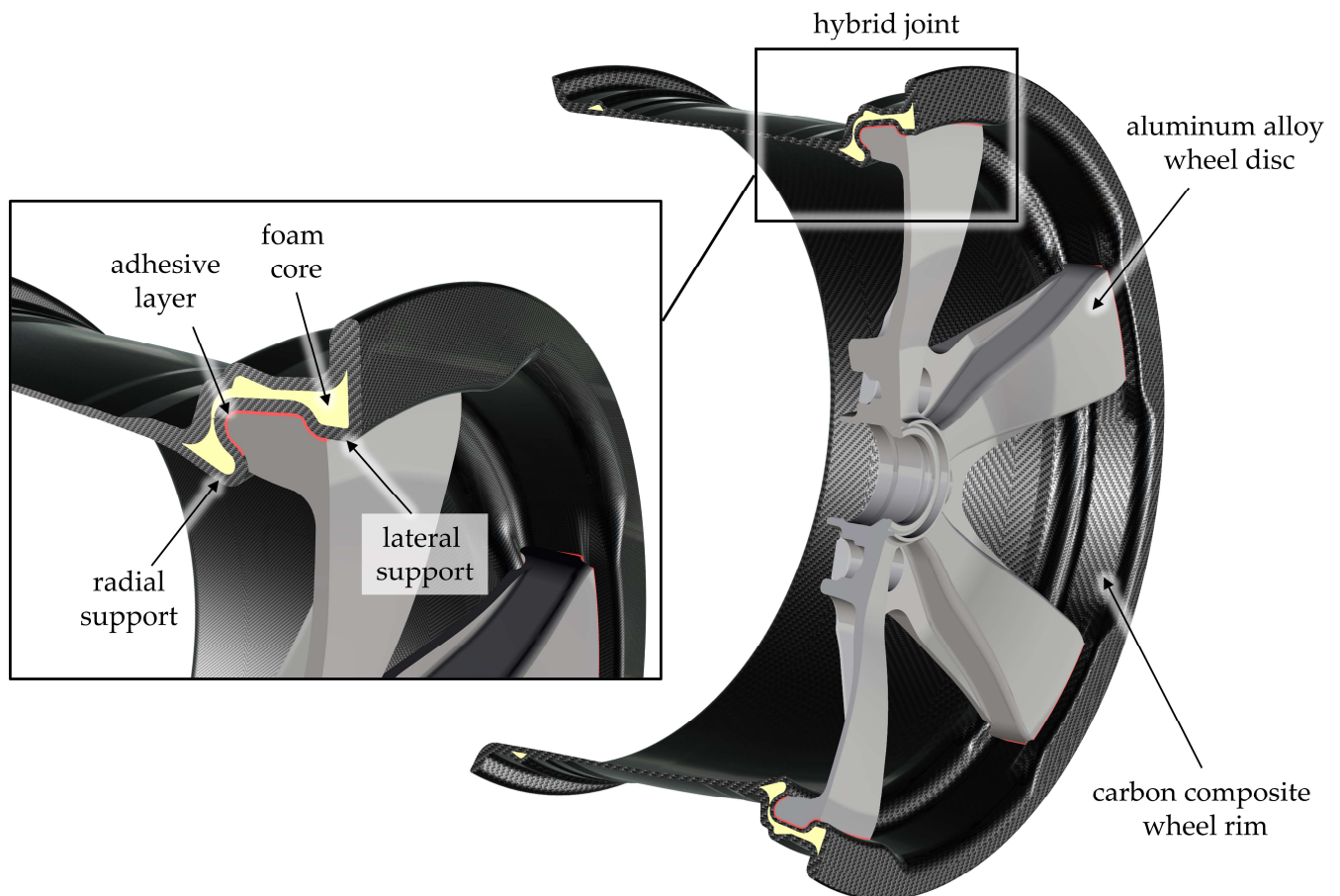

Figure 5. Form-fitted adhesive joint for the hybrid wheel, containing a radial and lateral support.

2.4.3. Manufacturing Concept

The least critical force resultants occur in the circumferential direction (Tables 3 and 4). Therefore, this degree of freedom is chosen as the bonding direction in which the adhesive bond without a form-fitted lock is considered sufficient. In the developed assembling process, the aluminum wheel disc is fixed on a rotation axis. The disc part is first positioned in between the joint areas of the composite rim. After application of the adhesive, the aluminum disc is rotationally moved into its final position, creating the form-fitted adhesive bond, as visualized in Figure 6a. In order to assure sufficient distribution of the adhesive over the bonding area and the realization of a defined adhesive thickness, the joint is designed in a wedge shape, as shown in Figure 6b. When locking the aluminum disc into position, an out-of-plane contact pressure is inserted, generating an evenly distributed adhesive layer with a constant thickness.

The wedge shape of the joint also enables the manufacturing of the composite rim via resin transfer molding (RTM). The geometry in the joint area can be realized in a multi-part tool, in which the respective tool segment can be demounted in a rotational direction.
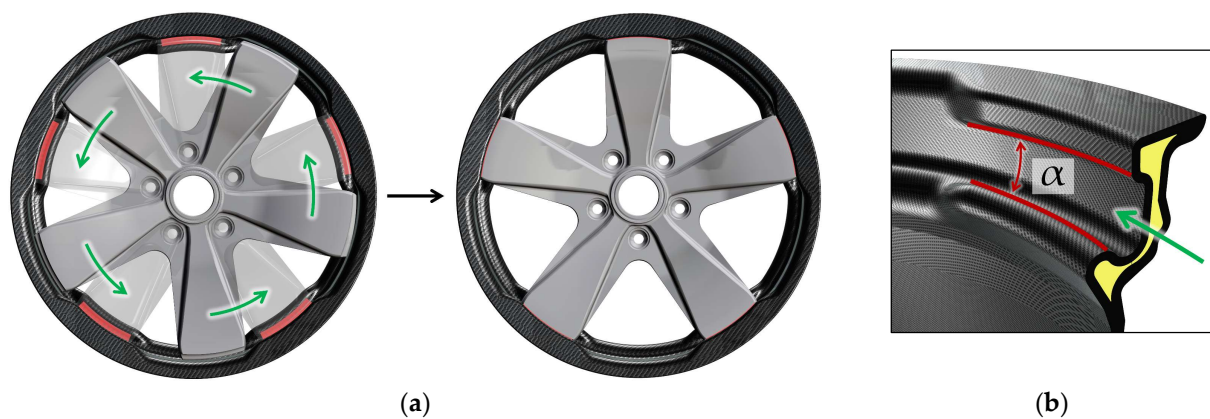
(**a**)　　　　　　　　　　　　　　　　　　　　　　　　　　　　　(**b**)

Figure 6. (**a**) Visualization of the bonding process in rotational direction (green arrow); (**b**) wedge shape (α) of the joint intersection.

3. Design and Manufacturing of Subcomponent Specimens

3.1. Design of Subcomponent Specimens

3.1.1. Geometrical Design of Subcomponent Specimen

Apart from the computational strength analysis of the joint, which may be presented in future publications, first, experimental validation of the joint performance is an important step in the preliminary design stage. Therefore, subcomponent specimens are designed, which represent the joint of an aluminum spoke with the composite rim, as shown in Figure 7a. The joint geometry is projected from the circular layout to a linear layout, reducing the manufacturing efforts of the subcomponent. However, the cross-sectional design with the foam core, as well as the bonding area and the wedge shape, stay similar to the joint design in the wheel. In order to demonstrate the benefit of the form-fitted adhesive design compared to a basic adhesive design, two variations of subcomponent specimen are realized, as shown in Figure 7b,c.
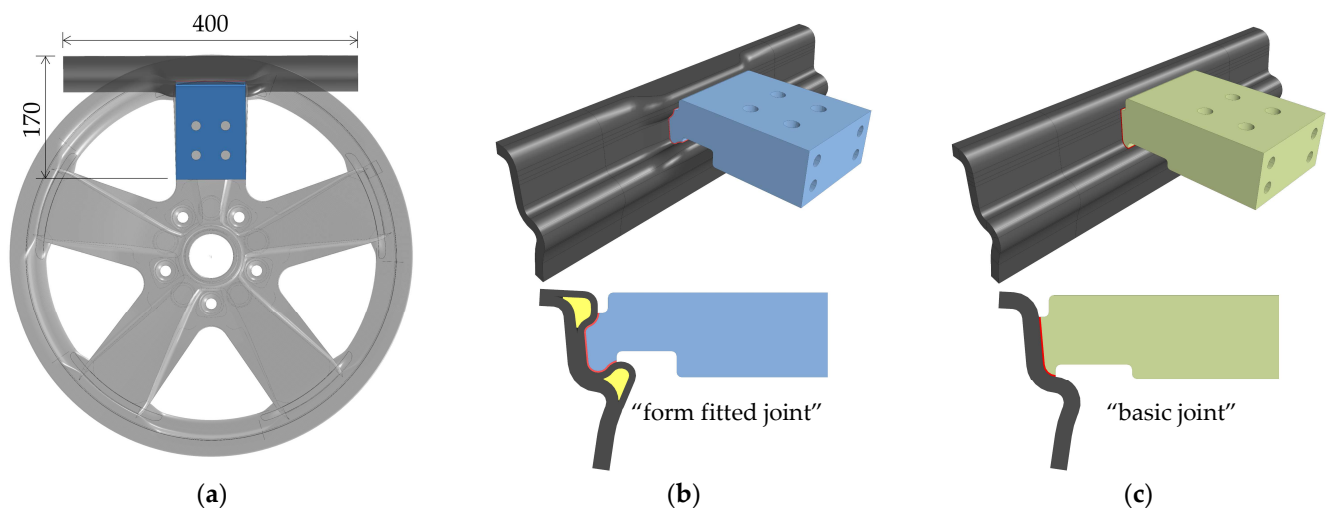

(**a**)　　　　　　　　　　　　　　　　(**b**)　　　　　　　　　　　　　　　　(**c**)

Figure 7. (**a**) Visualization of the subcomponent specimen as representation of the joint between the aluminum spoke and composite rim; (**b**) subcomponent specimen as a variation "form-fitted joint"; (**c**) subcomponent specimen as a variation "basic joint".

The interfaces of the specimens are designed in a way that they can be loaded in a test bench in a radial and a lateral orientation, as further described in Section 4.1. Both ends of the composite part can be fixed in a clamping device. The aluminum part can be joined to the test stand via bolted joints.

3.1.2. Comparative Evaluation of the Subcomponent Design

The subcomponent specimens represent a simplified design of the wheel joint, enabling a first experimental validation with comparatively little manufacturing and testing efforts. The finite element simulation of the basic joint in the wheel model and the subcomponent model enable a comparative evaluation.

The evaluated force and moment resultants are shown in Table 5. The radial loading of the subcomponent up to 7.47 kN shows similar resultants compared to the critical thermal load case of the wheel model. The lateral loading of the subcomponent up to −10.89 kN compared to the critical cornering load case of the wheel shows greater deviations of the radial force resultant and the circumferential moment resultant. However, it can be argued that the additional compressional radial loading of −9.25 kN in the wheel model has a supporting effect regarding lateral strength of the joint, due to the greater surface pressure.

Table 5. Force and moment resultants within the wheel joint for the thermal load cases, evaluated with the design adaptation in the rim flange.

Model	Load Case	Force Resultants			Moment Resultants		
		F_φ (kN)	F_R (kN)	F_L (kN)	M_φ (Nm)	M_R (Nm)	M_L (Nm)
subcomponent	radial loading: 7.47 kN	0	**7.47**	0.09	5	0	0
wheel	thermal: 23 °C to −40 °C	0	**7.47**	0.05	26	0	0
subcomponent	lateral loading: 10.89 kN	0.20	−0.86	**−10.89**	63	0	0
wheel	cornering: 180° position	0.13	−9.25	**−10.89**	136	11	−3

The comparative evaluation of the joint deformation for the exemplary radial load case is shown in Figure 8a,b. The composite part of the subcomponent specimen is designed with a specific resulting stiffness; thus, the deformation in the joint area in the model (0.39 mm) is roughly similar to the deformation in the wheel model (0.35 mm).
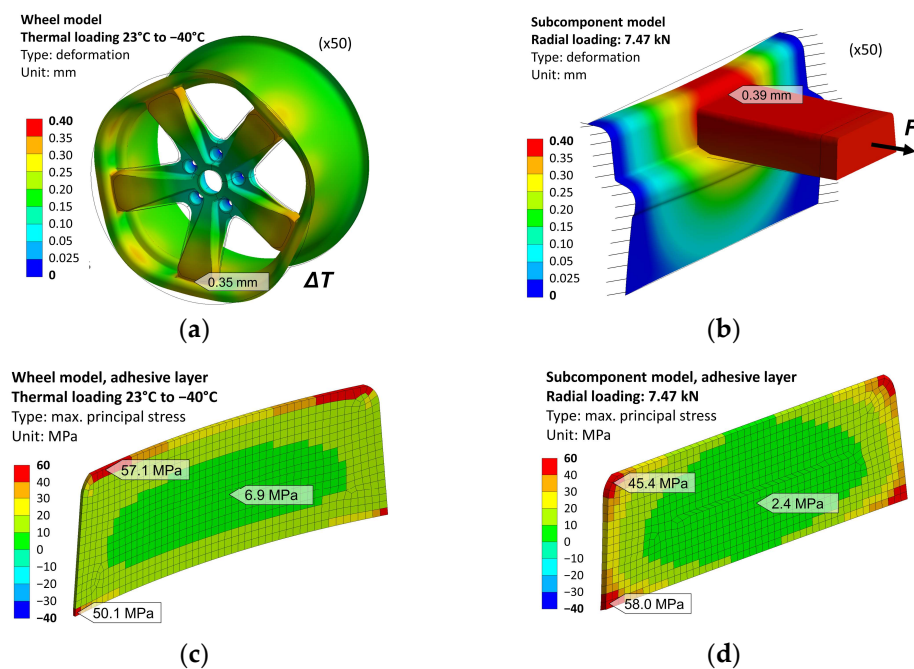

Figure 8. Comparative finite element analyses; (**a**) deformation of wheel; (**b**) deformation of subcomponent; (**c**) adhesive stresses in wheel; (**d**) adhesive stresses in subcomponent.

The comparative evaluation of the maximum principal stress in the adhesive layer for the exemplary radial load case is shown in Figure 8c,d. In both models, the adhesive

area and thickness are similar. However, the simplified linear layout, as well as the difference in stiffness of the aluminum adherend, lead to a slightly different stress state in the subcomponent model, with more pronounced stresses up to 58.0 MPa at the bottom corners and less pronounced stresses of 2.4 MPa in the center. Still, the deviations are considered acceptable for the objective of first experimental validation with subcomponents. More realistic validations can be generated by tests on wheel prototypes after a detailed design stage.

3.2. Manufacturing of Subcomponent Specimens

The manufacturing of subcomponent specimens is performed in several different steps. The composite adherend is realized via a vacuum infusion process. Therefore, the dry layup, including the woven fabrics and the foam core segments, is placed into a mold and sealed with a vacuum bag, as shown in Figure 9a. The resin is then infused into the mold cavity by a vacuum pump. For the curing process of the resin, the specimens are placed in an oven at 120 °C for 40 min and then at 190 °C for 2 h. In Figure 9b, a cross-sectional cut of the "form-fitted" composite adherend with its foam core is shown.
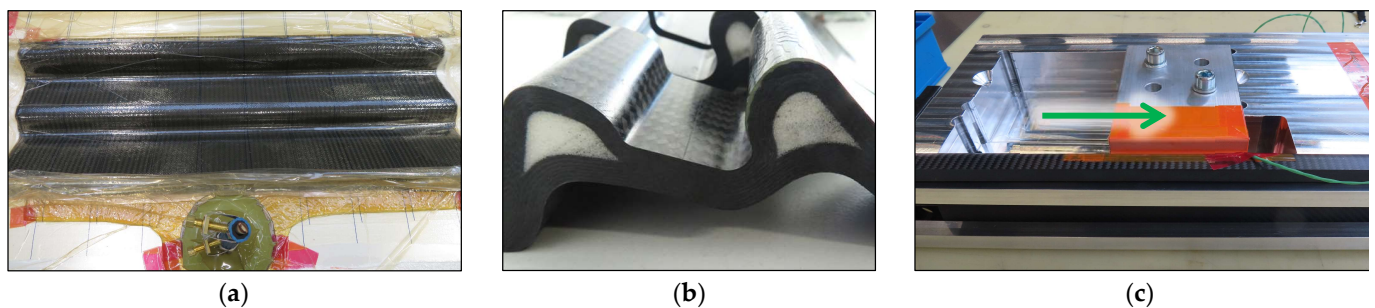

| (a) | (b) | (c) |

Figure 9. Manufacturing of subcomponent specimens: (**a**) vacuum infusion process of composite adherend; (**b**) cross-sectional view of form-fitted composite adherend; (**c**) bonding process (green arrow) within a mounting tool.

The aluminum adherend is made from a forged aluminum alloy within a milling and drilling process. For the adhesive bonding process, a mounting tool is realized, as shown in Figure 9c. Here, the adherends are joined in a similar bonding direction as planned for the wheel joint, creating contact pressure via the wedge-shaped form of the interfaces. For the curing process of the adhesive, the assembly is exposed to 180 °C for 30 min. Figure 10 shows the finished subcomponent specimens in variations such as "basic joint" and "form-fitted joint".

| (a) | (b) |

Figure 10. Subcomponent specimens as (**a**) "basic joint"; (**b**) "form-fitted joint".

4. Experimental Analysis of Subcomponent Specimens

The objective of the tests on subcomponent specimens is a first experimental evaluation of the performance of the joint design. Therefore, a test bench is realized, a test program is defined, and the test results are discussed. The main aspects of the investigations are the following:

- Can the joint withstand the required maximum loading?
- What are the failure modes of the joint?
- How does the "form-fitted joint" perform compared to the "basic joint"?
- What is the influence of temperature on the joint performance?

4.1. Test Bench

For the experimental evaluation of the joint, a test bench is realized, which allows for the testing of the joint in different load cases and at different temperatures. Figure 11a shows the CAD design of the test bench with its main components. The specimen can be mounted in a clamping device, connecting the composite side of the specimen to a fixed support. The loads are introduced on the aluminum side of the specimen by a hydraulic cylinder with a maximum limit of 25 kN. The movement of the cylinder is guided by a linear carriage. The specimen is placed within a climate chamber, so that loading at different temperatures can be realized by a hot-air unit. The resulting forces can be measured by a 3D load cell, placed outside the climate chamber. The displacement as well as the temperature are measured close to the adhesive joint.
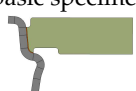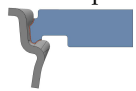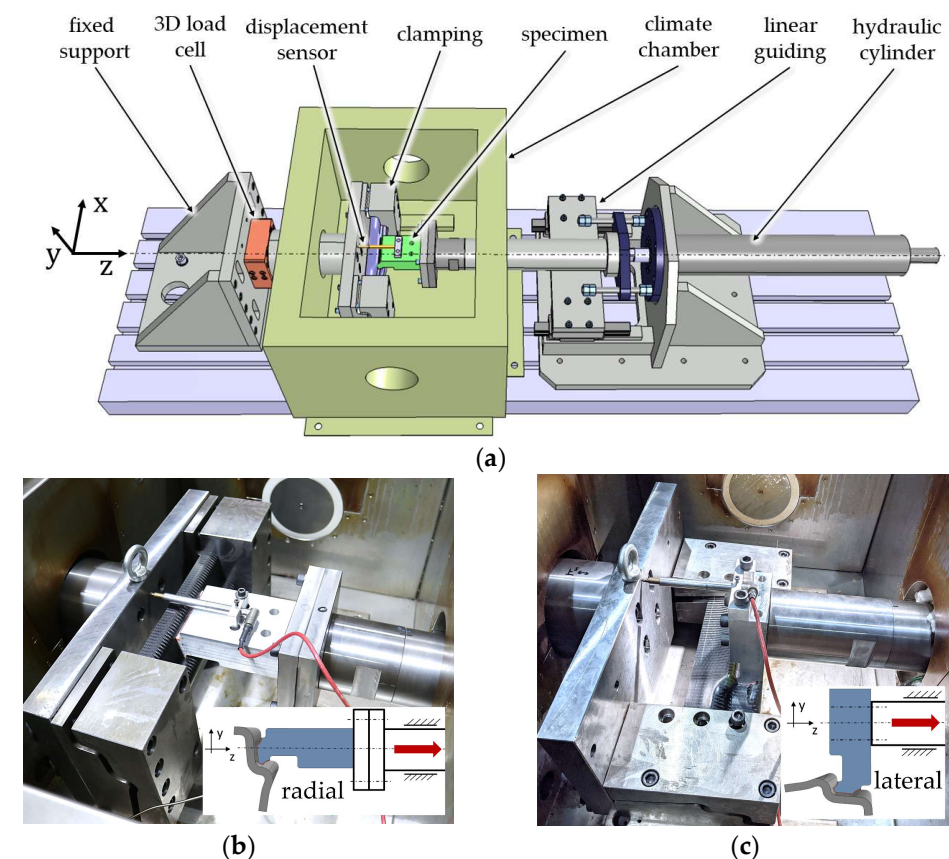

Figure 11. (**a**) CAD design of the test bench for the experimental evaluation of subcomponent specimens; (**b**) radial orientation of the specimen within the test bench; (**c**) lateral orientation.

The specimens can be mounted in two different orientations, as shown in Figure 11b,c. In the first orientation, the load can be introduced in the radial direction of the joint; in the second orientation, the load is introduced in the lateral direction.

4.2. Test Program

The selected test program is shown in Table 6. Due to a limited number of specimens, the test parameters are limited to two variations of specimens ("basic" and "form-fitted"), two load cases (radial and lateral), and two temperatures (23 and 150 °C). Each parameter set contains a sample size of two to three specimens. The load is applied as quasi-static loading, with a constant displacement of 1 mm/min.

Table 6. Test program for subcomponent specimens with different load cases and temperatures.

Specimens	Type of Test	Load Case	Number of Specimens 23 °C	Number of Specimens 150 °C
"basic specimen"	quasi-static test	radial	3	2
		lateral	3	2
"form-fitted specimen"	quasi-static test	radial	3	3
		lateral	3	3
	residual fatigue test	radial	1	
		lateral	1	

On two specimens, a residual fatigue test is performed under tension/tension loading with a stress ratio of $R = 0.1$ and a frequency of 4 Hz.

4.3. Test Results and Discussion

4.3.1. Quasi-Static Tests

The test results of the quasi-static tests on the subcomponent specimens are shown in Figures 12 and 13 as force–displacement curves. For each test, a first-crack initiation, located at the edge of the adhesive layer, can be identified in the trend of the curve and confirmed by the visual observation of a video recording of the test. After a phase of crack propagation, total failure of the specimens occurs as a rupture. However, due to the limit of the hydraulic cylinder at 25 kN, some specimens are not tested until total failure.
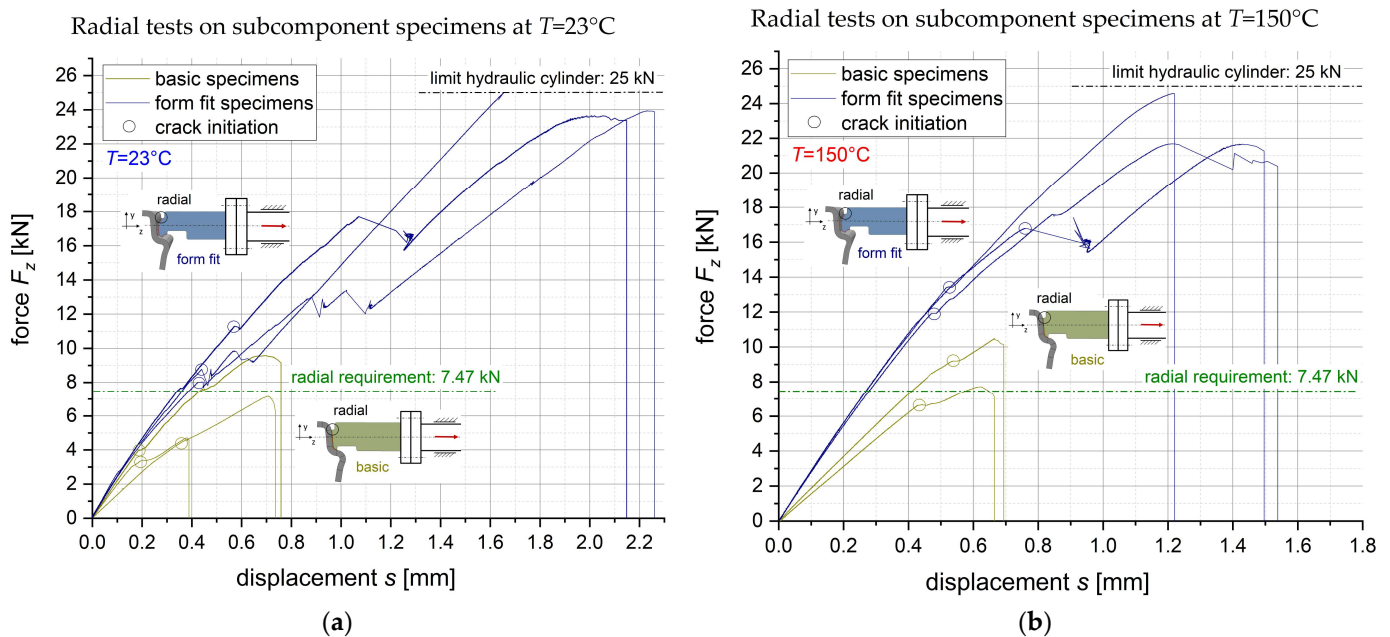

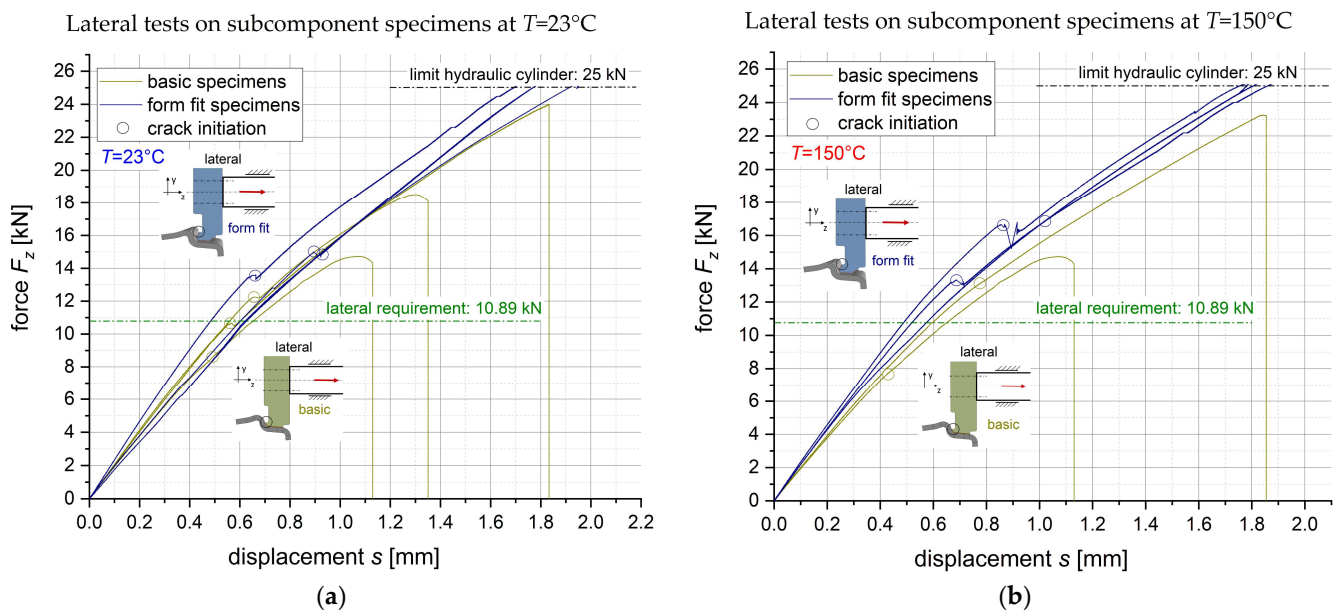**Figure 12.** Force–displacement curves of radial tests on subcomponent specimens: (**a**) 23 °C; (**b**) 150 °C.

Figure 13. Force–displacement curves of lateral tests on "basic" and "form-fitted" subcomponent specimens at (**a**) 23°C; (**b**) 150°C.

The test results of the radial load case are shown in Figure 12a for 23 °C and Figure 12b for 150 °C. For both temperatures, the results show significant improvement of the maximum bearable force of the "form-fitted joint" compared to the "basic joint". The crack initiation of the "form-fitted joint" occurs after the required radial load of 7.47 kN (Table 4), while the "basic joint" does not meet the requirement.

Table 7 shows the adherends after total failure with their characteristic failure patterns. At 23 °C, the failure predominantly occurs in the surface layer of the composite adherend, due to the high out-of-plane stresses in the radial load case. At 150 °C, the failure pattern shows more pronounced cohesive failure within the adhesive layer.

Table 7. Characteristic failure pattern in radial tests for the "basic joint" and the "form-fitted joint".

	$T = 23\ °C$	$T = 150\ °C$
basic joint		
form-fitted joint		

The test results of the lateral load case are shown in Figure 13a for 23 °C and Figure 13b for 150 °C. Similar to the radial tests, the "form-fitted joint" shows improved performance regarding strength at crack initiation as well as total failure, compared to the "basic joint". For both temperatures, the required maximum lateral load of 10.89 kN (Table 3) is met by the "form-fitted joint". Table 8 shows the facture pattern of the "basic joint" from the lateral tests with predominant cohesive failure within the adhesive layer. For the "form-fitted joint", rupture does not occur within the range of 25 kN of the hydraulic cylinder. However, the visual crack observation indicates a failure mode within the composite surface layer.

Table 8. Characteristic failure pattern in the lateral test for the "basic joint".

	T = 23 °C		*T* = 150 °C	
basic joint				
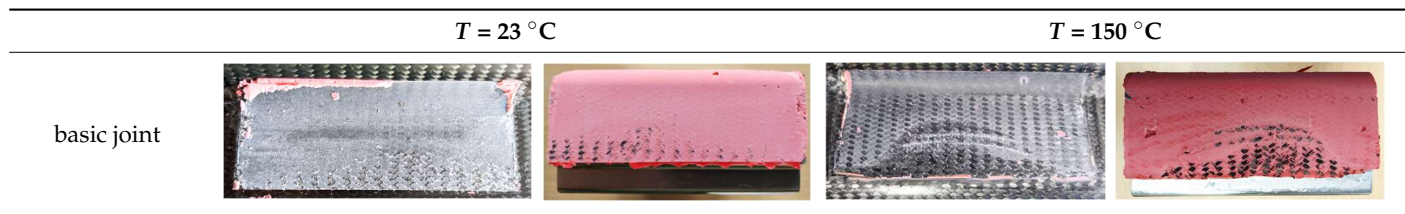
For both load cases, radial and lateral, the variations in temperatures of 23 and 150 °C do not show significant influences in absolute strength of the joint. Still, variations in failure modes occur, with predominant failure of the composite surface layer at 23 °C and predominant cohesive failure within the adhesive layer at 150 °C. This indicates different effects of temperature influence for the composite adherend and the adhesive, which have been observed in other studies in the review of literature [19,20].

The distinctive phase of crack propagation before total failure of the "form-fitted joint" indicates a high margin of safety after crack initiation. In addition, further design optimization of the adhesive edge, which has been identified in the literature [18], might result in further improvement of the joint strength. However, the low sample size and the scattering of the test results need to be considered.

4.3.2. Residual Fatigue Tests

For each load case, one of the "form-fitted specimens", which did not rupture after 25 kN quasi-static loading, is tested in a residual fatigue test at a very high maximum load of 24 kN at 23 °C. The specimen under cyclic radial loading fails after 5639 cycles, and the specimen under cyclic lateral loading fails after 691,763 cycles. This preliminary fatigue evaluation indicates good fatigue strength of the joint.

5. Conclusions

Within this research, an adhesive joint for a hybrid automotive wheel is developed, joining the aluminum wheel disc with the composite wheel rim. The development includes the analysis of joint requirements, the generation of a joint design and the experimental evaluation of the joint performance in tests on subcomponent specimens.

The structural joint requirements are obtained via a finite element simulation of the hybrid wheel in different load cases (Table 1). The force and moment resultants at the interface between the aluminum spoke and composite rim are evaluated, identifying several critical load combinations (Table 3).

Within a design phase considering different design parameters from the literature, an adhesive joint design is developed (Figure 5), which offers a lightweight potential of 6% compared to a conventionally bolted wheel design, and which contains two main characteristics:

- The adaption of the fiber layup in the composite rim flange, which reduces the radial force resultants during the thermal load cases significantly;
- The geometrical joint design with a form-fitted radial and lateral support

For the experimental evaluation of the joint design, subcomponent specimens (Figure 10) are manufactured. The specimens represent the joint of the aluminum spoke with the composite rim and are realized in two variations, as a "basic joint" and as a "form-fitted joint". The experimental evaluation offers the following conclusions:

- The newly developed "form-fitted joint" meets the required critical radial and lateral load and shows significant strength increasement compared to the "basic joint".
- After a first-crack initiation, the joint shows a distinctive crack propagation phase before final rupture, offering advantages regarding safety design.

- The variation in temperature influences the failure mode of the joint, with a predominant failure of the composite surface layer at 23 °C and a more pronounced cohesive failure within the adhesive layer at 150 °C.
- Residual fatigue tests on the subcomponent specimens indicate good fatigue strength.

The experimental evaluation shows promising results regarding the structural performance of the joint design. However, further investigations within a detailed design phase and experimental phase need to be carried out:

- optimization via detailed structural analyses of adhesive and adherend failure;
- optimization of the joint design regarding crack initiation at the edge of the adhesive;
- further evaluation of critical load cases in multiaxial loading at different temperatures with a larger sample size of specimens;
- fatigue tests on wheel prototypes.

Author Contributions: Conceptualization, J.-D.W., T.K., H.L., J.D. and S.B.; methodology, J.-D.W., T.K., J.D. and S.B.; validation, J.-D.W. and J.D.; formal analysis, J.-D.W.; investigation, J.-D.W. and T.K.; data curation, J.-D.W.; writing—original draft preparation, J.-D.W.; writing—review and editing, T.K., H.L., J.D., A.J., O.H. and S.B.; visualization, J.-D.W.; supervision, J.D. and S.B.; project administration, T.K. and S.B.; funding acquisition, J.D. and S.B. All authors have read and agreed to the published version of the manuscript.

Conflicts of Interest: The authors declare no conflict of interest.

References

1. Hybrid Composite Wheel Reduces Fuel Consumption. Available online: https://www.reinforcedplastics.com/content/products/hybrid-composite-wheel-reduces-fuel-consumption/ (accessed on 4 January 2023).
2. Every Gram Counts-M Carbon Compound Wheels for the BMW M4 GTS. Available online: https://www.bmw-m.com/en/topics/magazine-article-pool/every-gram-counts.html (accessed on 4 January 2023).
3. Wheels from the Highest Standard-Mubea Performance Wheels. Available online: https://www.mubea.com/en/mubea-performance-wheels (accessed on 4 January 2023).
4. CFK-Räder Gehen 2016 in Serie. Available online: https://www.kfz-betrieb.vogel.de/cfk-raeder-gehen-2016-in-serie-a-505562/ (accessed on 4 January 2023).
5. Porsche and the Braided Carbon Fiber Wheel. Available online: https://www.compositesworld.com/articles/porsche-and-the-braided-carbon-fiber-wheel (accessed on 4 January 2023).
6. Rondina, F.; Taddia, S.; Mazzocchetti, L.; Donati, L.; Minak, G.; Rosenberg, P.; Bedeschi, A.; Dolcini, E. Development of full carbon wheels for sport cars with high-volume technology. *Compos. Struct.* **2018**, *192*, 368–378. [CrossRef]
7. Wacker, J.-D.; Laveuve, D.; Contell Asins, C.; Büter, A. Design of a composite nose wheel for commercial aircraft. *IOP Conf. Ser. Mater. Sci. Eng.* **2021**, *1024*, 012018. [CrossRef]
8. The Fuchsfelge-Forged, Not Cast. Available online: https://www.fuchsfelge.com/en/the-fuchsfelge.html (accessed on 4 January 2023).
9. Thyssenkrupp Carbon Components GmbH. Vehicle Wheel Comprising a Wheel Rim and a Wheel Disc. Patent WO2016/037611A1, 17 March 2016.
10. Mubea Carbo Tech GmbH. Wheel for a Vehicle. Patent WO2016/066769A1, 6 May 2016.
11. GOHybrid-Gestaltung und Optimierung von Hybridverbindungen unter Besonderer Berücksichtigung der Unterschiedlichen Wärmedehnungen der Werkstoffpartner. Available online: https://www.werkstoffplattform-hymat.de/Group/GOHybrid/Pages (accessed on 4 January 2023).
12. Da Silva, L.F.M.; Öchsner, A.; Adams, R.D. *Handbook of Adhesion*, 2nd ed.; Springer: Berlin/Heidelberg, Germany, 2011; pp. 2–4.
13. Marques, E.A.S.; da Silva, L.F.M.; Banea, M.D.; Carbas, R.J.C. Adhesive Joints for Low- and High-Temperature Use: An Overview. *J. Adhes.* **2015**, *7*, 556–585. [CrossRef]
14. Mubea Carbo Tech GmbH. Heat Shield Structure for a Wheel. Patent WO2016/097159A1, 17 March 2016.

15. Carbon Revolution PTY Ltd. Method of Producing Thermally Protected Composite. Patent WO2016/168899A1, 27 October 2016.

16. Shang, X.; Marques, E.A.S.; Machado, J.J.M.; Carbas, R.J.C.; Jiang, D.; da Silva, L.F.M. Review on techniques to improve the strength of adhesive joints with composite adherends. *Compos. Part B Eng.* **2019**, *177*, 107363. [CrossRef]

17. Wacker, J.-D.; Tittmann, K.; Koch, I.; Laveuve, D.; Gude, M. Fatigue life analysis of carbon fiber reinforced polymer (CFRP) components in hybrid adhesive joints. *Mater. Sci. Eng. Technol.* **2021**, *52*, 1230–1247. [CrossRef]

18. Qin, G.; Na, J.; Tan, W.; Mu, W.; Ji, J. Failure prediction of adhesively bonded CFRP-Aluminum alloy joints using cohesive zone model with consideration of temperature effect. *J. Adhes.* **2019**, *95*, 723–746. [CrossRef]

19. *ASTM D5573−99*; Standard Practice for Classifying Failure Modes in Fiber-Reinforced-Plastic (FRP) Joints. ASTM International: West Conshohocken, PA, USA, 2019.

20. *ISO 11003-2:2019-06*; Adhesives-Determination of Shear Behaviour of Structural Adhesives-Part 2: Tensile Test Method Using Thick Adherends. International Organization for Standardization: London, UK, 2019.

21. *ISO 527-5:2009*; Plastics-Determination of Tensile Properties-Part 5: Test Conditions for Unidirectional Fibre-Reinforced Plastic Composites. DIN Deutsches Institut für Normung e.V.: Berlin, Germany, 2009.

22. *ISO 4587:2003-03*; Adhesives-Determination of Tensile Lap-Shear Strength of Rigid-to-Rigid Bonded Assemblies. DIN Deutsches Institut für Normung e.V.: Berlin, Germany, 2003.

23. OTTO FUCHS KG. EN AW-6082 nach DIN EN 573 FUCHS AS15/AS11. Product Data Sheet, Rev. 1. Available online: https://www.otto-fuchs.com/fileadmin/user_upload/Infocenter/Werkstoffinformationen/Al-Datenblaetter/AS10-15.pdf (accessed on 4 January 2023).

24. WELA Handelsgesellschaft mbH. Kohlefasergewebe WELA GG-245-1000T (AKSA A-38). Product Data Sheet. 2020. Available online: https://wela-hamburg.de/wp-content/uploads/2019/01/datenblatt.pdf (accessed on 4 January 2023).

25. WELA Handelsgesellschaft mbH. UD-Kohlefasergewebe WELA GV-303-0500UTFX. Product Data Sheet. 2013. Available online: https://wela-hamburg.de/faserverstaerkungen/ (accessed on 4 January 2023).

26. Huntsman Advanced Materials. Araldite®LY 1560/Aradur®917-1/Accelerator DY 079. Product Data Sheet. 2016. Available online: https://www.huntsman-transportation.com/EN/products/all-products/composite-resin-systems.html/ (accessed on 4 January 2023).